

Elucidation of the electronic structure of semiconducting single-walled carbon nanotubes by electroabsorption spectroscopy

Hongbo Zhao* and Sumit Mazumdar

Department of Physics, University of Arizona, Tucson, Arizona 85721, USA

(Dated: July 2, 2018)

We report benchmark calculations of electroabsorption in semiconducting single-walled carbon nanotubes to provide motivation to experimentalists to perform electroabsorption measurement on these systems. We show that electroabsorption can detect continuum bands in different energy manifolds, even as other nonlinear absorption measurements have failed to detect them. Direct determination of the binding energies of excitons in higher manifolds thereby becomes possible. We also find that electroabsorption can provide evidence for Fano-type coupling between the second exciton and the lowest continuum band states.

PACS numbers: 73.22.-f, 78.67.Ch, 71.35.-y

Semiconducting single-walled carbon nanotubes (S-SWCNTs) are being intensively investigated because of their unique properties and broad potential for applications [1, 2]. Recent theoretical investigations have emphasized the strong role of electron-electron interactions and the consequent excitonic energy spectra in S-SWCNTs [3, 4, 5, 6, 7]. While within one-electron theory two-photon absorption (TPA) begins at the same energy threshold as the lowest one-photon absorption, exciton theories predict a significant energy gap between the lowest two-photon exciton and the optical exciton [8, 9]. This energy gap gives the lower bound to the binding energy of the lowest exciton, and has been determined experimentally [8, 9, 10, 11]. Exciton theories of S-SWCNTs therefore may be considered to have firm footing.

We note, however, that existing experiments have focused almost entirely on the lowest exciton and information on the *overall energy spectra* of S-SWCNTs is severely limited. To begin with, no signature of even the lowest continuum band is obtained from such experiments. Equally importantly, finite diameters of S-SWCNTs lead to subband quantization and consequently a series of energy manifolds labeled $n = 1, 2, \dots$, etc. with increasing energies (see Fig. 4 in Ref. [9]), and although emission studies detect the optical exciton in the $n = 2$ manifold (*Ex2*) [12], it has not been possible to determine its binding energy. TPA or transient absorption techniques used to determine the binding energy of the optical exciton in the $n = 1$ manifold (*Ex1*) are not useful for this purpose, as nonlinear absorptions to states in the $n = 2$ manifold will be masked by the strong linear absorption to *Ex1* (this is particularly true here as the energy of *Ex1* is nearly half that of the states in the $n = 2$ manifold). Interference effects between *Ex2* and the $n = 1$ continuum band, suggested from relaxation studies of *Ex2* [13, 14], are also difficult to verify directly. Clearly, measurements that can probe much broader energy regions of S-SWCNTs are called for.

In the present Letter, we propose electroabsorption

(EA), which measures the difference between the absorption $\alpha(\omega)$ with and without an external static electric field, as the ideal technique for understanding the overall energy spectra of S-SWCNTs. EA has provided valuable information on both conventional semiconductors [15] and π -conjugated polymers [16, 17, 18]. The similarity in the energy spectra of π -conjugated polymers and S-SWCNTs [7, 9] makes EA particularly attractive. EA spectroscopy of S-SWCNTs has already been attempted [19], while continuous wave photomodulation spectroscopy has been interpreted as electroabsorption caused by local electric fields [20]. EA measurements are currently difficult as complete separation of semiconducting from metallic SWCNTs has not been possible to date. Recent advances in the syntheses of chirality enriched S-SWCNTs [21] strongly suggest that EA measurements will become possible in select S-SWCNTs in the near future. We present here benchmark calculations of EA for several wide nanotubes that give new insights to their electronic structures, and provide the motivation for and guidance to experimental work.

As in our previous work [7, 9] we choose the semiempirical π -electron Pariser-Parr-Pople (PPP) model [22] as our field-free Hamiltonian,

$$H_0 = - \sum_{\langle ij \rangle, \sigma} t_{ij} (c_{i\sigma}^\dagger c_{j\sigma} + c_{j\sigma}^\dagger c_{i\sigma}) + U \sum_i n_{i\uparrow} n_{i\downarrow} + \frac{1}{2} \sum_{i \neq j} V_{ij} (n_i - 1)(n_j - 1). \quad (1)$$

Here $c_{i\sigma}^\dagger$ creates a π -electron with spin σ on the i th carbon atom, $\langle ij \rangle$ implies nearest neighbors, $n_{i\sigma} = c_{i\sigma}^\dagger c_{i\sigma}$ is the number of π -electrons with spin σ on the atom i , and $n_i = \sum_{\sigma} n_{i\sigma}$ is the total number of π -electrons on the atom. The parameter t_{ij} is the one-electron hopping integral, U is the repulsion between two π -electrons occupying the same carbon atom, and V_{ij} the intersite Coulomb interaction. We have chosen Coulomb and hopping parameters as in our recent work [7]. In principle, we should also include the electron-phonon interactions

[6], since EA spectra for real materials will contain signatures arising from phonon sidebands [16]. This, however, will make the EA calculations much too complicated. In agreement with prior EA experiments on π -conjugated polymers [16], our calculations here find that EA signals due to excitons and continuum bands are sufficiently different that there can be no confusion in distinguishing between exciton sidebands and continuum bands.

We are interested in optical absorptions polarized parallel to the nanotube axis and consider only the component of the static electric field along the same direction. The overall Hamiltonian is written as [17]

$$H = H_0 + eFz = H_0 + \mu F, \quad (2)$$

where e is the charge of the electron, F the field strength along the nanotube axis (taken to be the z -direction), and μ the transition dipole operator along z .

The EA is calculated in two steps [17]. We first diagonalize H_0 in the space of all single excitations from the Hartree-Fock ground state, using the single-configuration interaction (SCI) approximation [7]. Eigenstates of S-SWCNTs are of even (A_g) or odd (B_u) parity, and dipole matrix elements are nonzero only between states of opposite parity [23]. We calculate the field-free absorption spectra $\alpha(\omega; 0)$ from the calculated dipole matrix elements between the ground $1A_g$ state and excited B_u states [7, 9]. We now evaluate the matrix elements of μ between *all* excited states of H_0 , construct and diagonalize the total Hamiltonian H with the eigenstates of H_0 as the basis states, and calculate the new absorption $\alpha(\omega; F)$. The EA is given by $\Delta\alpha(\omega; F) = \alpha(\omega; F) - \alpha(\omega; 0)$.

The effect of the nonzero field is to mix A_g and B_u states. Within second order perturbation theory appropriate for weak fields, $Ex1$ undergoes a Stark energy shift ΔE_{Ex1} , given by

$$\Delta E_{Ex1} = \sum_j \frac{|\langle Ex1 | \mu | j A_g \rangle|^2 F^2}{E_{Ex1} - E_{j A_g}}, \quad (3)$$

where the sum over A_g states includes the $j = 1$ ground state. In addition, A_g excitons that are forbidden for $F = 0$ become weakly allowed for $F \neq 0$. This transfer of oscillator strengths between A_g and B_u excitons is also quadratic in F . Nondegenerate perturbation theory cannot, however, describe the mixing of A_g and B_u states belonging to continuum bands and the EA in these energy regions can be only calculated numerically. As we discuss below, the same is true for $Ex2$, which is buried within the $n = 1$ continuum. We have ignored the dark excitons [6, 7] in our discussion, as they play no role in linear or nonlinear absorption.

We first describe the $n = 1$ energy region separately. In Fig. 1(a) we have plotted the calculated linear absorption along with EA spectrum in the energy range corresponding to the $n = 1$ manifold for $F = 10$ kV/cm for the

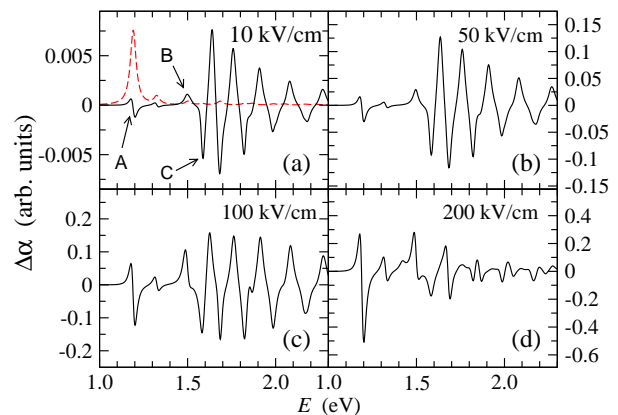


FIG. 1: (Color online) (a) Linear absorption (red), and EA spectrum of the (10,0) S-SWCNT in the $n = 1$ energy region for $F = 10$ kV/cm. (b)–(d) EA spectra for $F = 50, 100,$ and 200 kV/cm, respectively.

(10,0) S-SWCNT. Figs. 1(b)–(d) show the EA spectra for $F = 50, 100,$ and 200 kV/cm, respectively. EA for other S-SWCNTs, including chiral ones, are similar. The three most important features of the EA spectra are indicated in Fig. 1(a). The derivative like feature A corresponds to the redshift of $Ex1$. From Eq. (3), the redshift (as opposed to a blueshift) is the consequence of the existence of an A_g two-photon exciton that is closer in energy to $Ex1$ than the $1A_g$ ground state, and that also has a stronger dipole coupling to $Ex1$ [17]. In analogy to π -conjugated polymers [17], we have previously referred to the two-photon exciton state as the mA_g [9]. It is this state that is visible in TPA and transient absorption [8, 9, 10, 11]. Feature B in Fig. 1(a) corresponds to the field-induced absorption to the mA_g . Feature C is a dip in the absorption due to the B_u state at the threshold of the $n = 1$ continuum band (hereafter the nB_u [9]). The continuum band is recognized by its oscillatory nature, and its appearance over a broad energy region where there is no linear absorption. EA can therefore give the binding energy of $Ex1$ directly, as the energy difference between the features C and A.

The amplitude of the continuum band signal in Fig. 1 is much larger than that of the exciton at low field. This has been observed previously in a crystalline polydiacetylene [16]. Finite conjugation lengths prevent the observation of the continuum band EA signal in disordered noncrystalline π -conjugated polymers [18], but this signal will be observable in S-SWCNTs where the tubes are known to be long. Features due to the exciton and the continuum can be distinguished easily even when electron-phonon interactions lead to sidebands, from their different field dependence [16]. In Fig. 2(a) we show that the calculated field dependence of both the energy shift of $Ex1$ and the amplitude of EA signal due to $Ex1$ for (6,5), (7,6), and (10,0) S-SWCNTs are quadratic in F up to the largest

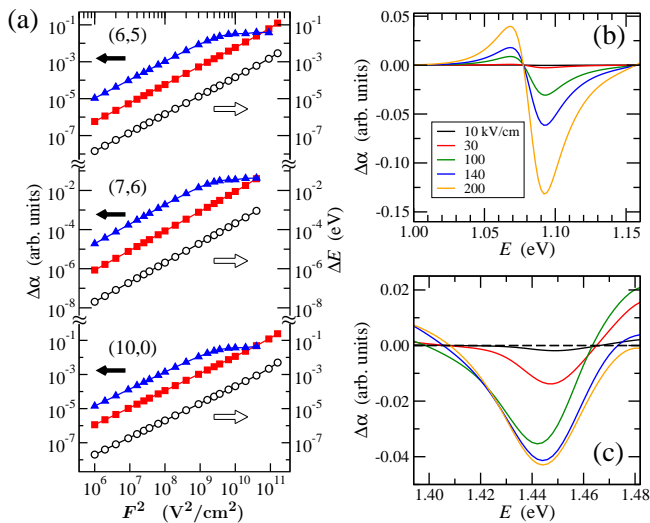


FIG. 2: (Color online) (a) Field dependence of ΔE_{Ex1} (open circles), the EA amplitude of $Ex1$ (solid squares) and nB_u (solid triangles) for the (6,5), (7,6), and (10,0) S-SWCNTs. (b) and (c) Field dependence of EA signals for the (6,5) S-SWCNT due to the $Ex1$ and the nB_u , respectively.

value of F . EA amplitudes due to the nB_u , also plotted in the figure, exhibit weaker dependence on F at strong fields, in agreement with that observed in the crystalline polydiacetylenes [16]. In Figs. 2(b) and (c) we have plotted EA signals due to $Ex1$ and the nB_u , respectively, at different fields. EA due to the continuum (but not the exciton) exhibits the expected band-broadening [16] as a function of the field.

We now discuss EA over the entire energy region, focusing on the $n = 2$ manifold. In Fig. 3(a) we have shown the calculated linear absorption for the (6,5) S-SWCNT, while Fig. 3(b) shows the EA spectrum for $F = 50$ kV/cm. The EA spectrum is dominated by two distinct and slowly decaying oscillating signals due to the $n = 1$ and 2 continuum bands. Comparison of Figs. 3(a) and (b) indicates that $Ex2$ lies within the $n = 1$ continuum. We also note that the signal due to $Ex2$ is much stronger than that due to $Ex1$. This is a consequence of the interference between $Ex2$ and the $n = 1$ continuum, as we prove by comparing the true EA of Fig. 3(b) with that in Fig. 3(c), where the coupling between $Ex2$ and the $n = 1$ continuum states has been artificially eliminated. We calculated EA from the $n = 1$ manifold states alone by removing all $n = 2$ states from Eq. (2); similarly the calculation of EA from the $n = 2$ states ignored the $n = 1$ states. Fig. 3(c) shows the superposition of these two independent EAs. The very small EA signal due to $Ex2$ in Fig. 3(c) is completely obliterated by the smooth envelope of the $n = 1$ continuum, clearly indicating that the much larger signal in Fig. 3(b) is a consequence of the coupling between $Ex2$ and the $n = 1$ continuum states. We have further verified this by performing the

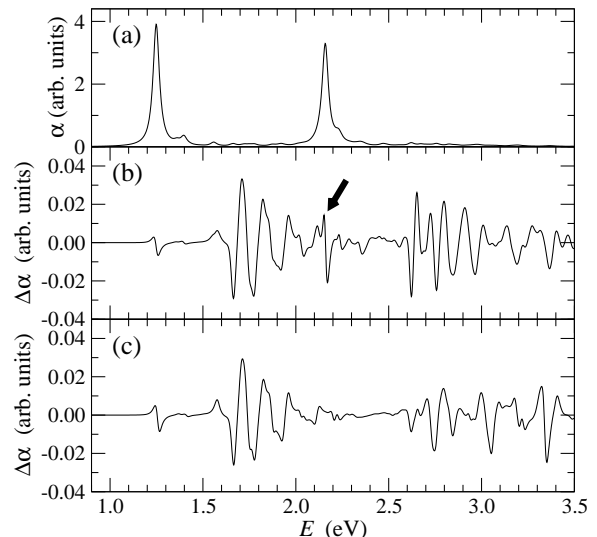


FIG. 3: Linear absorption (a) and EA spectrum (b) in the energy region covering both $n = 1$ and 2 energy manifolds for the (6,5) S-SWCNT for $F = 50$ kV/cm. The arrow indicates $Ex2$. (c) Superposition of the EAs for the $n = 1$ and 2 energy manifolds, calculated separately and independently of one another, at the same field.

EA calculations with varying U/t : larger Coulomb interactions imply larger Coulomb coupling between $Ex2$ and the $n = 1$ continuum, and give larger EA signal for $Ex2$. We have observed these characteristics in our calculated EA spectra for all S-SWCNTs.

Coulomb coupling between a discrete state with a continuum leads to the well-known Fano resonance, which manifests itself as a sharp asymmetric line in the linear absorption [24]. Calculation of the absorption spectrum of the (8,0) S-SWCNT has previously found this coupling [4]. In contrast to this standard description of the Fano effect, the interference effect we observe in the EA spectrum is a consequence of transition dipole coupling between $Ex2$ and the $n = 1$ continuum states. One interesting consequence of this dipole coupling is that unlike $Ex1$, which undergoes redshift in all cases, $Ex2$ can be either redshifted [as observed in our calculations for (6,4), (7,6), and (11,0) S-SWCNTs] or blueshifted [observed for (6,2), (8,0), and (10,0) S-SWCNTs]. The reason for this is explained in Table I, where we have listed for the (8,0) and the (6,4) S-SWCNTs the dominant transition dipole couplings between $Ex2$ and A_g states along with the energy differences between them. Among these states, only one is from the $n = 2$ manifold, which is the mA_g2 state, the equivalent of the mA_g state in the $n = 2$ manifold. All other states belong to the $n = 1$ continuum. The relatively large energy difference between the mA_g2 and $Ex2$, comparable to that between the mA_g and $Ex1$, indicates that the energy shift of $Ex2$ is *determined predominantly by the dipole-coupled $n = 1$ continuum states*. States below and above $Ex2$ contribute to blue and red

TABLE I: Dominant transition dipole couplings between $Ex2$ and A_g states, as well as the corresponding energy differences. The mA_g2 state is labeled with an asterisk (*).

| (n,m) | $\langle Ex2 \mu jA_g\rangle/\langle Ex2 \mu 1A_g\rangle$ | $E_{Ex2} - E_{jA_g}$ (eV) |
|---------|---|---------------------------|
| (8,0) | 8.31* | -0.423 |
| | 8.01 | 0.057 |
| | 6.22 | -0.103 |
| | 1.22 | 0.073 |
| (6,4) | 15.3 | 0.049 |
| | 11.5 | -0.051 |
| | 11.1 | 0.081 |
| | 9.64 | -0.070 |
| | 9.45 | -0.080 |
| | 6.62 | -0.025 |
| | 6.45* | -0.402 |

shifts, respectively, and the energy differences in Table I rationalize blue (red) shift in the (8,0) ((6,4)) S-SWCNT. The *magnitude* of the energy shift of $Ex2$ in all cases is smaller than that of $Ex1$ because of partial cancelations, even as the amplitude of the EA signal of $Ex2$ is larger.

Correlated SCI eigenstates of the Hamiltonian (1) are superpositions of band-to-band excitations from the Hartree-Fock ground state. Furthermore, within the non-interacting tight-binding model as well as within Hartree-Fock theory, matrix elements of the component of the transition dipole moment along the nanotube axis are nonzero only for ‘‘symmetric’’ excitations, viz., from the highest valence band to the lowest conduction band, from the second highest valence band to the second lowest conduction band, etc. Hence the strong dipole couplings between $Ex2$ and proximate $n = 1$ continuum eigenstates of A_g symmetry *necessarily implies that $Ex2$ eigenstate contains basis vector components belonging to both $n = 1$ and $n = 2$ manifolds*. This is precisely the signature of Fano coupling. Table II shows the relative weights of the $n = 1$ one electron-one hole excitations in the correlated $Ex2$ eigenstates of several S-SWCNTs. These contributions are chirality-dependent, and reach as high as 30%.

The EA due to the $n = 2$ continuum in Fig. 3(b) is similar to that of the $n = 1$ continuum. The threshold of the $n = 2$ continuum is always detectable in our calculated EA spectra. Further confirmation of the band edge can come from measurements of its field-dependence, which is the same as for $n = 1$. Taken together with emission measurements that give the energy location of $Ex2$ [12], EA can then give the precise binding energy of $Ex2$.

In conclusion, we have performed benchmark calcula-

TABLE II: Relative weights of Hartree-Fock $n = 1$ excitations in the SCI $Ex2$ eigenstate of several S-SWCNTs.

| | (8,0) | (10,0) | (6,2) | (6,4) | (6,5) | (7,6) | (9,2) |
|------------|-------|--------|-------|-------|-------|-------|-------|
| percentage | 3% | 2% | 23% | 12% | 20% | 33% | 26% |

tions showing that EA measurements in S-SWCNTs can provide valuable information on their electronic structures that are difficult to obtain from other measurements. In particular, EA spectroscopy can detect both $n = 1$ and 2 continuum bands. EA due to continuum bands can be easily differentiated from those due to excitons. Precise estimates of the binding energies of both $Ex1$ and $Ex2$ can therefore be obtained. $Ex1$ is predicted to have a redshift, which would provide indirect evidence for the mA_g state detected in complementary nonlinear absorption measurements [8, 9, 10, 11]. High resolution will also allow direct detection of the mA_g . We find strong evidence for Fano-type coupling between $Ex2$ and $n = 1$ continuum states that has previously been suggested from the experimental observation of ultrafast nonradiative relaxation of $Ex2$ [13, 14]. EA measurements can provide a more direct evidence for this. Syntheses of chirality enriched S-SWCNTs are allowing a variety of sophisticated spectroscopic measurements. The results reported here provide strong motivation for EA spectroscopy of S-SWCNTs. It is tempting to extend the current EA calculations to the $n = 3$ energy region. Although the $n = 3$ exciton is identifiable from linear absorption calculations, our calculations indicate that its coupling to the $n = 2$ continuum states is even stronger than that of $Ex2$ with the $n = 1$ continuum. The analysis of excitons and continuum bands become rather complicated at these high energies. Work is currently in progress along this direction.

This work was supported by NSF-DMR-0406604.

* Current address: Department of Physics, University of Hong Kong, Hong Kong, China

- [1] P. L. McEuen, M. S. Fuhrer, and H. Park, IEEE Trans. Nanotechnol. **1**, 78 (2002).
- [2] J. Chen *et al.*, Science **310**, 1171 (2005).
- [3] T. Ando, J. Phys. Soc. Jpn. **66**, 1066 (1997); *ibid*, **73**, 3351 (2004).
- [4] C. D. Spataru *et al.*, Phys. Rev. Lett. **92**, 077402 (2004); Appl. Phys. A **78**, 1129 (2004).
- [5] E. Chang *et al.*, Phys. Rev. Lett. **92**, 196401 (2004).
- [6] V. Perebeinos *et al.*, Phys. Rev. Lett. **92**, 257402 (2004); *ibid* **94**, 027402 (2005).
- [7] H. Zhao and S. Mazumdar, Phys. Rev. Lett. **93**, 157402 (2004); Z. Wang, H. Zhao, and S. Mazumdar, Phys. Rev. B **74**, 195406 (2006).
- [8] J. Maultzsch *et al.*, Phys. Rev. B **72**, 241402 (2005).
- [9] H. Zhao *et al.*, Phys. Rev. B **73**, 075403 (2006).
- [10] F. Wang *et al.*, Science **308**, 838 (2005).
- [11] G. Dukovic *et al.*, Nano Lett. **5**, 2314 (2005).
- [12] S. M. Bachilo *et al.*, Science **298**, 2361 (2002).
- [13] C. Manzoni *et al.*, Phys. Rev. Lett. **94**, 207401 (2005).
- [14] Z. Zhu *et al.*, preprint (2006).
- [15] D. E. Aspnes, Phys. Rev. **147**, 554 (1966); *ibid*, **153**, 972 (1967).
- [16] G. Weiser and Á. Horváth, in *Primary Photoexcitations*

in Conjugated Polymers: Molecular Exciton versus Semiconductor Band Model, edited by N. S. Sariciftci (World Scientific, Singapore, 1998), pp. 318–362.

- [17] D. Guo *et al.*, Phys. Rev. B **48**, 1433 (1993).
- [18] M. Liess *et al.*, Phys. Rev. B **56**, 15712 (1997).
- [19] J. W. Kennedy *et al.*, cond-mat/0505071.
- [20] C. Gadermaier *et al.*, Nano Lett. **6**, 301 (2006).
- [21] M. S. Arnold *et al.*, Nat. Nanotechnol. **1**, 60 (2006); R. Krupk *et al.*, Science **301**, 344 (2003); V.W. Brar *et al.*, J. Nanosci. Nanotechnol. **5**, 209 (2005).
- [22] R. Pariser and R. G. Parr, J. Chem. Phys. **21**, 466 (1953); J. A. Pople, Trans. Faraday Soc. **49**, 1375 (1953).
- [23] This is only approximately true for chiral NTs, but in practice there is no difference between zigzag and chiral; see Ref. [7].
- [24] U. Fano, Phys. Rev. **124**, 1866 (1961).